# TRIAXIAL STRESS STATES AND PUNCHING SHEAR IN SLABS OF A FIBRE REINFORCED ULTRA HIGH STRENGTH CEMENT-BASED COMPOSITE

Gert Heshe, M.Sc., Senior Lecturer, Department of Building Technology and Structural Engineering, University of Aalborg, Sohngaardsholmsvej 57, DK-9000 Aalborg, Denmark

Claus V. Nielsen, M.Sc., NUC-Research and Development Institute, Niels Jernes Vej 10, DK-9220 Aalborg Ø, Denmark

ABSTRACT

Tests on 100 × 200 mm cylinders under triaxial stress states and punching shear test on slabs are reported. The material of the cylinders and slabs is the COMPRESIT matrix. COMPRESIT matrix reported here is an ultra high strength cement-based steel fibre reinforced composite. The results from the triaxial tests are compared with similar tests on ordinary concrete, high strength concrete and the Coulomb failure criterion. The tests show that the Coulomb failure criterion is a reasonable failure criterion for the COMPRESIT-matrix as for ordinary concrete. Formulas for a failure criterion following the test results are derived.

A plastic upper bound solution is proposed to predict the ultimate punching shear load. The test results obtained from experiments, where the span-depth ratio of the slabs is varied, are used to fit the theoretical model by means of two effectiveness factors.

Key words: COMPRESIT, composite, triaxial stress states, failure criterion, steel fibres, plasticity, punching shear.

## 1. INTRODUCTION

COMPRESIT is a new type of very strong, ductile and rigid materials which has been invented by H. H. Bache and further developed at Aalborg Portland A/S, Denmark.

COMPRESIT is a structural material built up of a very strong and brittle cementitious matrix, toughened with a high concentration of fine steel fibres – 6% by volume – and further reinforced with a high concentration of deformed steel bars. Tests have been carried out on beams with a flexural reinforcing ratio of more than 13%, cf. /5/.

The COMPRESIT matrix has the following composition given in % by weight: Densit binder (Portland Cement, Silica fume, admixtures) 34,4%, quarts sand 43.0%, water 6.1% and steel fibres 16.5%

The above composition gives a water/binder ratio of 0.18 by weight. The diameter and length of tbe steel fibres are 0.15 and 6 mm respectively.

Further information about the COMPRESIT material or CRC as it was originally termed, and the composition of the COMPRESIT matrix can be found in /1/, /2/, /3/, /4/, /5/ and /6/.

The research on COMPRESIT has been going on since 1986 and deals with the basic properties of the materials.

In this paper we will concentrate on triaxial compression tests and punching shear tests performed on the COMPRESIT matrix.

## 2. COMPRESIT MATRIX UNDER TRIAXIAL STRESS STATES

### 2.1 Theoretical background

The methods to calculate the bearing capacity of COMPRESIT elements are nearly the same as to calculate the bearing capacity of reinforced concrete elements.

Advances in the design of concrete structure are placing an ever increasing emphasis on the need for knowledge concerning the strength of concrete subjected to generalized stresses.

For concrete the first failure criterion was formulated by Coulomb in 1773. Later on more complicated criteria were formulated, but very often the Coulomb criterion is still used partly because of the simplicity of the criterion and partly because for the most cases of practical interest the Coulomb criterion has an accuracy well within normal engineering accuracy.

The results from triaxial compression tests with cylinders of the COMPRESIT matrix will in the following be compared with the Coulomb failure criterion.

With only compression the Coulomb failure criterion predicts a sliding failure /7/ given by

$$| \tau | = c - \sigma \tan \varphi \tag{1}$$

where $c$ is the cohesion, $\varphi$ is the friction angle, $\sigma$ is a normal stress counted positive as a tensile stress and $\tau$ is a shear stress. Equation (1) can be transformed into a relation between the lowest and the highest of the principal stresses $\sigma_3$ and $\sigma_1$, respectively, and will then have the following appearance

$$k\sigma_1 - \sigma_3 = 2\sqrt{k}\, c = f_c \tag{2}$$

$f_c$ is the numerical value of the uniaxial compression strength of the COMPRESIT matrix and

$$k = \frac{1 + \sin\varphi}{1 - \sin\varphi} \tag{3}$$

## 2.2 Test specimens and test equipments

The test specimens were 24 cylinders with the dimensions 100 × 200 mm and the material was COMPRESIT matrix with the composition given in section 1.

The test specimens were cured after the following programme: 1 day in mould, 28 days in water at 20°C, 5 days wrapped in plastic and placed in a timber box under transportation from Aalborg Portland to the Department of Structural Engineering, Technical University of Denmark, at a temperature about 10°C, and finally about 65 days in laboratory with 20°C and 60-65% relative air humidity.

Under these conditions the uniaxial compressive strength of the cylinders was about 165 MPa.

In order to avoid excentricity the ends of the cylinders were grounded accurately plane and parallel.

Strain gauges were aligned symmetrically about the centre circumference of the test specimens to measure axial and circumferential strain. Two gauges placed diametrically opposite to each other were used for each direction.

Due to the expected large values of strains special strain gauges were manufactured. The strain gauges used were a post-yielding wire gauges calibrated until 20% strain. The mesh length was 60 mm and the electrical resistance was 120 Ω.

The test specimens were stressed in a high pressure triaxial cell type WS 40040.

The general arrangement of the triaxial cell is shown in figure 1. It consists essentially of a base unit, a barrel section enclosing the pressure chamber, a piston to apply axial load, and a retaining cap, all of which are machined to close tolerances from maraging steel. In the pressure chamber the confining oil pressure can rise to max. 140 MPa and with the piston an axial load of 5,000 kN can be superimposed from a 10,000 kN hydraulic compression test machine, a Walther and Bai product.

The test equipment is described in details in /8/.

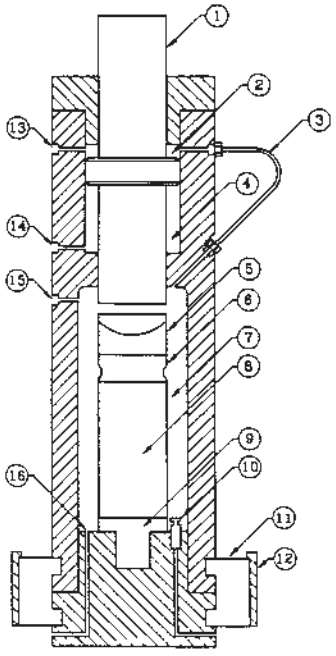

1: Balanced piston
2: Upper oilchamber
3: Connecting oilpipe
4: Lower oilchamber
5: Top cap
6: Top plate (pore pressure outlet)
7: Main oilchamber
8: Concrete specimen
9: Base plate (pore pressure outlet)
10: Electrical outlet
11: Clamp
12: Clamp ring
13: Deairing port A
14: Deairing port B
15: Deairing port C
16: Oilpressure inlet

Figure 1: General arrangement of the hydraulic triaxial cell, (from /8/).

To avoid oil entrance into the test specimens an impermeable sheath of a 1 mm soft synthetic oil resistant rubber material (Nitril rubber) with a shore hardness of 60-65° was used. The sheaths were glued together with a Neotal glue along a generatrix with an overlap of 20 mm. Normally, 2 sheaths per cylinder were used, but with high values of the confining pressures 3 sheaths were necessary.

### 2.3 Test execution and results

The tests were carried out at the Department of Structural Engineering, Technical University of Denmark. In order to compare the test results with the Coulomb failure criterion in a $\sigma_1 - \sigma_3$ diagram it was planned to determine 8 points $(\sigma_1, \sigma_3)$ with the following values of the confining pressure $\sigma_1$: 0, 20, 40, 60, 80, 100, 120 and 140 MPa. 3 cylinders were used to determine each point $(\sigma_1, \sigma_3)$.

When the prescribed confining pressure is obtained in the pressure chamber, giving hydrostatic pressure in the test specimen, the axial load is increased until failure. The stresses were increased corresponding to about 0.7 MPa/sec.

### 2.4 Test results and discussion

Table 1 shows corresponding mean values of the ultimate axial force $P_u$, the confining pressure $\sigma_1$, the axial stress $\sigma_3$ with belonging standard deviation $s$ and coefficient of variation $v$ and curing time. The numerical values of the stresses are used.

Table 1: The mean values of the ultimate axial force, the confining pressure $\sigma_1$, the axial stress $\sigma_3$ with the belonging standard deviation $s$ and the coefficient of variation $v$ and curing time. Numerical values are used.

| Test specimens No. | Mean value of the confining pressure $\sigma_1$ | Ultimate axial force $P_u$ | Mean value of the axial stress $\sigma_3$ | Standard deviation $s$ | Coefficient of variation $v$ | Curing time |
|---|---|---|---|---|---|---|
| | MPa | kN | MPa | MPa | % | days |
| 1–3 | 0 | 0 | 165.0 | 0.83 | 0.50 | 97 |
| 4–6 | 20.7 | 2216,0 | 302.8 | 3.34 | 1.10 | 96 |
| 7–9 | 40.4 | 2643.1 | 377.0 | 6.87 | 1.82 | 98 |
| 10–12 | 60.2 | 3008.3 | 443.2 | 5.94 | 1.34 | 101 |
| 13–15 | 80.0 | 3230.3 | 491.3 | 0.99 | 0.20 | 103 |
| 16–18 | 100.1 | 3396.7 | 532.5 | 5.85 | 1.10 | 97 |
| 19–21 | 120.2 | 3748.2 | 597.4 | 7.92 | 1.33 | 109 |
| 22–24 | 140.0 | 4146.2 | 667.9 | 11.52 | 1.72 | 102 |

For the confining pressure $\sigma_1 = 20{,}7$ MPa the coefficient of variation is 1.6%. For other values of $\sigma_1$ $v$ is smaller than 0.4%.

The confining pressure $\sigma_1$ is the highest principal stress, and the axial stress $\sigma_3$ is the

lowest principal stress. The middle principal stress $\sigma_2 = \sigma_1$. The stresses are counted positive as tensile stresses.

The axial stress $\sigma_3$ is calculated as

$$\sigma_3 = \sigma_1 - \frac{4 \cdot P_u \cdot 10^3}{\pi^2 \cdot 100^2} = \sigma_1 - 0.127 P_u \tag{4}$$

with $\sigma$ in MPa when $P_u$ in kN.

In figure 2 the test results are shown as a $\sigma_1/f_c - \sigma_3/f_c$ relationship. The numerical values of $\sigma_1$ and $\sigma_3$ are used.

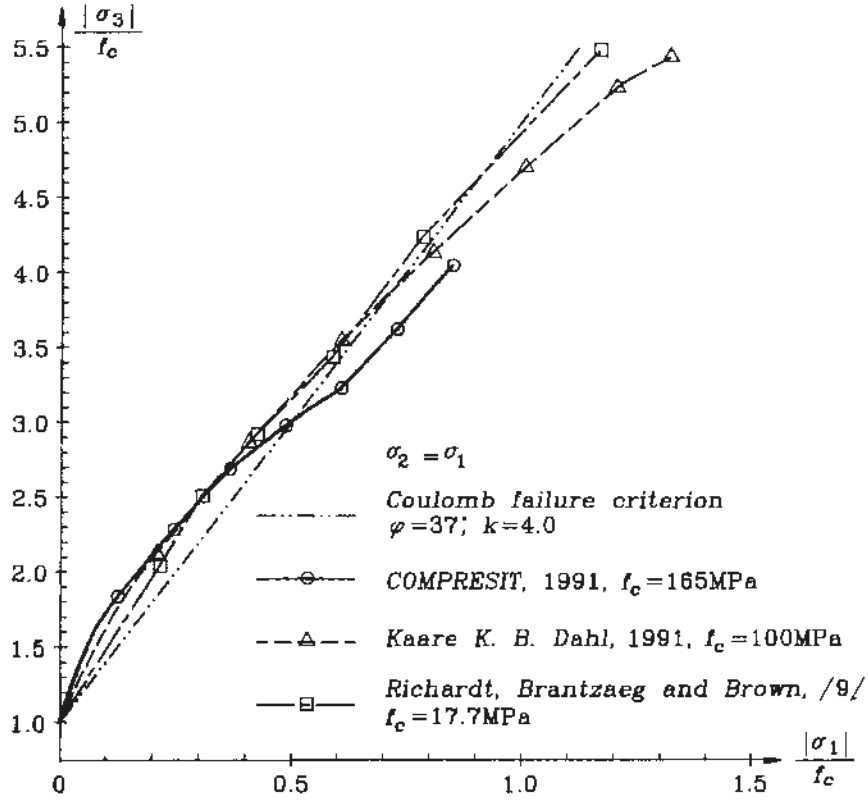


Figure 2: Dimensionless test results.

Figure 2 also shows test results from Kaare K. B. Dahl, 1991, Department of Structural Engineering, Technical University of Denmark, with high strength concrete ($f_c$ = 106 MPa), from Richardt, Branzaeg and Brown ($f_c$ = 17,7 MPa), /15/, and the straight line representing the Coulomb failure criterion corresponding to a friction angle $\varphi \approx 37°$ ($k$ = 4) which are normally used for ordinary concrete.

The Coulomb failure criterion for sliding failure given in (2) can be written as

$$k\frac{\sigma_1}{f_c} - \frac{\sigma_3}{f_c} = 1 \tag{5}$$

The COMPRESIT-curve in figure 2 can be composed of two curves fitting the test results:

a parabolic curve

$$\left(\frac{|\sigma_3|}{f_c} - 0.801\right)^2 = 9.64\,\frac{|\sigma_1|}{f_c} \qquad 0 < \frac{|\sigma_1|}{f_c} \leq 0.6 \tag{6}$$

a straight line

$$\frac{|\sigma_3|}{f_c} = 1.17 + 3.39 \cdot \frac{|\sigma_1|}{f_c} \qquad 0.6 \leq \frac{|\sigma_1|}{f_c} < 0.85 \tag{7}$$

From figure 2 it is seen that for small values of $|\sigma_1|/f_c$ the Coulomb failure criterion will give smaller values for $|\sigma_3|/f_c$ than the described tests. The opposite is the fact for big values of $|\sigma_1|/f_c$.

For increasing values of $f_c$ the value of $|\sigma_1|/f_c$ where the test curves cross the Coulomb curve will decrease.

The COMPRESIT test curve cross the Coulomb curve at about $|\sigma_1|/f_c = 0.5$.

At $(|\sigma_1|/f_c\,;\,|\sigma_3|/f_c) = (0.61;\,3.23)$ there is a remarkable change in the COMPRESIT test curve. From that point to point (0.85; 4.05) the test curve is a straight line.

The abrupt change in the slope of the curve showing the $\sigma_1/f_c - \sigma_3/f_c$ relationship might indicate an experimental error, but in table 1 it is seen that the coefficient of variation $v$ is very small, max. 1.7% for the tests with the confining pressure 100, 120 and 140 MPa.

No defect is found in the compressive cell of the test machine measuring the compressive force in the range 3500-5000 kN. Therefore, experimental errors do not seem to be the explanation of the abrupt change in the slope of the curve showing the $\sigma_1/f_c - \sigma_3/f_c$ relationship for the COMPRESIT matrix.

With the test data from the triaxial compression tests with the COMPRESIT matrix the authors are at the time of writing not able to give an explanation for the special form of the curve for $|\sigma_1|/f_c$ values bigger than 0.6.

In order to evaluate the accuracy of the Coulomb failure criterion with $\varphi \approx 37°$ used on the COMPRESIT matrix, the mean square error of the test results in figure 2 compared to the Coulomb curve is calculated.

For the results of Richardt, Branzaeg and Brown this error is found to be 0.45, for the results with high strength concrete by Dahl it is 1.32 and for COMPRESIT the mean square error is found to be 0.51. Therefore, it is concluded that the Coulomb failure criterion is a reasonably good approach for the COMPRESIT matrix.

It is seen that the Coulomb failure criterion will be on the safe side for values of $|\sigma_1|/f_c$ smaller than 0.5, and on the unsafe side for values of $|\sigma_1|/f_c$ bigger than 0.5. If the Coulomb failure criterion has to be on the safe side in the interval $0 < |\sigma_1|/f_c < 0.85$ a value for the friction angle $\varphi = 34.4°$ has to be used.

A visuel inspection of the cylinders with the naked eye after failure showed inclined lines of rupture with an angle $\alpha$ between the line of rupture and the generatrix of the cylinder. After failure the cylinders were still coherent and the lines of rupture were very fine. For cylinders with confining pressure 120 and 140 MPa $\alpha$ was about 29°. For the confining pressure 40, 60, 80 and 100 MPa $\alpha$ was about 38°. For the confining pressure 20 MPa

no inclined lines of rupture were to be seen with the naked eye but with a microscope magnifying about 10 times a 40 mm long vertical crack running from the top of the cylinder was found.

In all examined cylinders there was furthermore a tendency to a horizontal plane of rupture visible as a line on the curved surface of the cylinders.

As mentioned the cylinders were equipped with strain gauges for measuring of longitudinal strains as well as transverse strains. Many of the strain gauges broke down and many of them gave misleading results, particularly for the longitudinal strains. Therefore, no stress-strain relationships are shown in this paper. The explanation for the unsuccessful strain measurements is that there were a lot of air voids in the curved surface of the cylinders. Before the strain gauges were mounted the curved surface was sand-blasted and the air voids were filled with a mixture of lime, cement and fine sand called Husfix. But the tests showed that the filling of the deep air voids with Husfix was not totally successful. Therefore, strain gauges across the air voids were pressed into the air voids and broke down or gave a misleading result. For more informative description of these facts the reader is directed to the main report /10/.

## 3. PUNCHING SHEAR TESTS ON COMPRESIT MATRIX

A test series of 46 experiments has been carried out on slabs loaded to punching shear failure. The failure loads are compared to theoretical upper bound values using the theory of plasticity.

### 3.1 Plasticity theoretical analysis

In this model it is assumed that the COMPRESIT matrix is an ideal-plastic material in both compression and tension. To compensate for the fact that the matrix do not act ideal-plastic the effectiveness factors $\nu$ and $\rho$ are introduced. These factors reduce the uniaxial compression and tension strengths to effective values:

$$\left.\begin{aligned} f_c' &= \nu f_c \quad , \quad (0 \leq \nu \leq 1) \\ f_t' &= \rho f_c \quad , \quad (0 \leq \rho \leq 1) \end{aligned}\right\} \tag{8}$$

where $f_c$ is the uniaxial compression strength of 100 × 200 mm cylinders.

In /7/ pp. 29-35 a detailed background for these effective values, together with a general description of plastic analysis used on concrete, is given.

Normally the Coulomb failure criterion, mentioned in section 2.1, together with a separation failure criterion and the normality condition are used to predict the plastic failure load.

Here we use a parabolic failure criterion as described in /12/. In figure 3 the two criteria are illustrated in a $\sigma - \tau$ diagram.

The reason why the parabolic relation is preferred instead of the modified Coulomb criterion is that it leads to a much simpler expression for the upper bound failure load. Further the solution in /12/ has fewer restrictions to its validity as shown later.

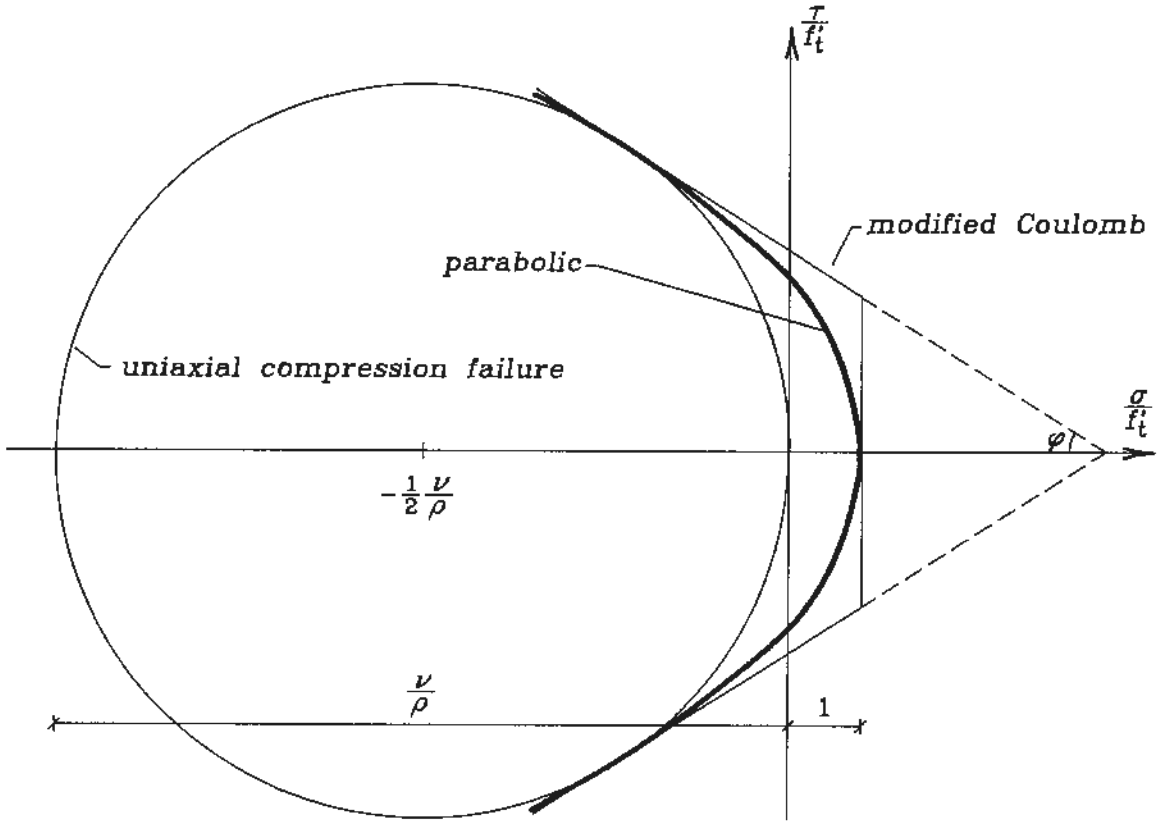


Figure 3: Failure criteria in dimensionless form.

The parabolic failure criterion shown in figure 3 has the following relation between normal and shear stresses on a failure surface

$$\frac{\sigma}{f_t'} = 1 - \frac{1}{4K}\left(\frac{\tau}{f_t'}\right)^2 \tag{9}$$

where $f_t'$ is the effective uniaxial tension strength of the matrix. The constant $K$ depends on the two effectiveness factors $\nu$ and $\rho$:

$$4K = \frac{\nu}{\rho} + 2\left(1 - \sqrt{\nu/\rho + 1}\right) \tag{10}$$

Using the work equation and a kinematically possible failure mechanism as shown in figure 4 an upper bound value of the ultimate punching shear load can be found, see /12/.

The most correct value of the ultimate load $P_u$ is found by minimizing with respect to the shape of the failure surface. Using variational principles it can be shown that the correct failure surface is given by the following expression

$$\frac{r}{h} = \frac{1}{2}\frac{d}{h}\left(\frac{d_1}{d}\right)^{x/h} \tag{11}$$

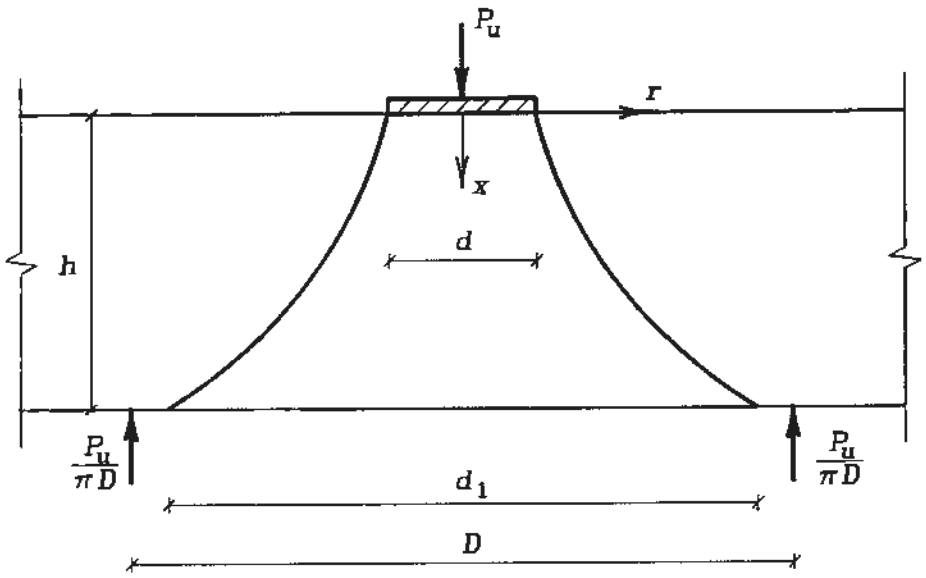


Figure 4: Rotationally symmetric failure surface for punching shear failure.

The punching diameter $d_1$ is calculated by use of iteration on the expression

$$\ln\left(\frac{d_1}{d}\right) = \frac{2\sqrt{K}}{d_1/h} \tag{12}$$

The ultimate load is given by the dimensionless expression

$$\frac{P_u}{\pi h^2 \nu f_c} = \frac{\rho}{\nu}\left(\frac{(d_1/h)^2 - (d/h)^2}{4} + \frac{2K}{\ln(d_1/d)}\right) \tag{13}$$

where the punching diameter $d_1$ is the smallest obtained from either (12) or $d_1 = D$.

In /12/ the load capacity given by (13) is shown to be nearly identical with the solution using the Coulomb criterion, /7/ pp. 366-370, and (13) is easier to use than the solution in /7/. Furthermore, (13) is valid for all values of $D/h > d/h$ while the solution in /7/ has the restriction $D/h \geq d/h + 2\tan\varphi$ where $\varphi$ is the friction angle (for ordinary concrete $\varphi \approx 37°$).

## 3.2 Experimental programme

In figure 5 a principal illustration of the test set-up is shown.

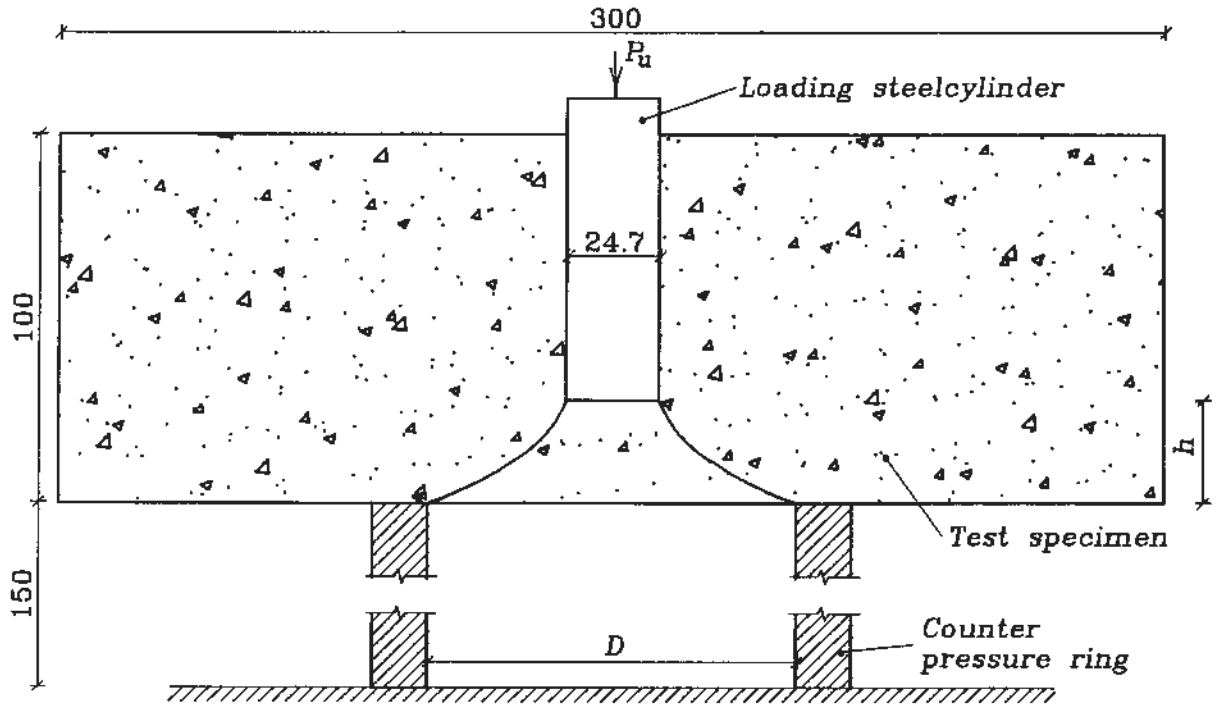


Figure 5: Cross-section of a rotation symmetric test specimen. All measures in mm.

The test specimens consist of slabs (300 × 300 × 100 mm) with a centrally placed circular hole. A steel cylinder with a diameter of $d = 24.7$ mm is placed in the hole and loaded until punching failure is registrated. To avoid friction between the sides of the steel cylinder and the slab the hole is made about 0.3 mm wider than the cylinder.

The reason for giving the slabs a depth of 100 mm which is more than the punching depth $h$ (= 25 and 50 mm) is to avoid a bending failure of the slab and ensure punching shear failure.

Furthermore, the relatively small dimensions of the specimens make the tests comparable to the so-called LOK-test as described in /13/ and the specimens can be fitted into a conventional testing machine.

The experiment is carried out in a 500 kN test machine (INSTRON 1255) which provides the necessary compression force $P$ on the loading cylinder. The specimen is placed on the base of the test machine supported by a cylindrical counter pressure ring with the inner diameter $D$.

During the test corresponding values of the compression force $P$ and the movement $\Delta$ of the steel cylinder relative to the upper surface of the specimen are registrated. In figure 6 is shown a photo of the test setup which shows the two transducers (LVDT) measuring $\Delta$.

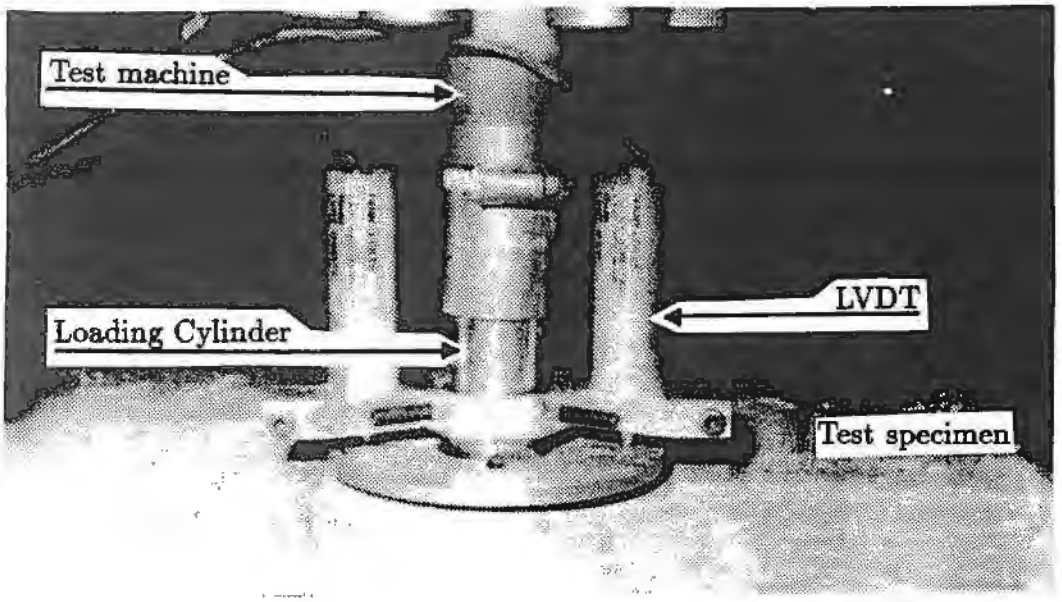


Figure 6: Test setup with loading cylinder and transducers.

The tests are carried out with a constant displacement rate at approximately 0.2 mm/min. of the rig of the test machine. In figure 8 different $P - \Delta$ relations are shown. After passing the peak value and $P$ has decreased to about 75% of the ultimate load, the rate is increased to approximately 1 mm/min.

### 3.2.1. Test specimens

Tests have been carried out with 46 test specimens. A survey of these specimens is shown in table 2. 43 test specimens are concreted with COMPRESIT matrix and to investigate the effect of the fibres 3 specimens are concreted without steel fibres. Furthermore 9 of the specimens are concreted with one or two layers of reinforcement bars. The parameters varied are the ratio $D/h$ and $d/h$, see figure 5. Two values of the depth $h$ (25 and 50 mm) and 7 values of the diameter $D$ of the counter pressure ring have been used which have resulted in 9 different values of the ratio $D/h$ as shown in table 2.

The specimens were cured 1 day in mould, 28 days in water at 20°C and finally about 45 days in laboratory at 20°C and 60-65% relative air humidity.

For all the specimens of type A the diameter $D$ is smaller than the undisturbed punching diameter $d_1$, see figure 4, while for specimens of type B and C the failure surface does not interact with the annular support, that is $d_1 < D$.

Table 2: Survey of the test specimens.

| Type of specimen | Number of specimens | $h$ mm | $D$ mm | $D/h$ | $d/h$ | Notes |
|---|---|---|---|---|---|---|
| A-1 | 5 | 25 | 62.5 | 2.5 | 1.0 | |
| A-2 | 6 | 25 | 100.0 | 4.0 | 1.0 | |
| A-3 | 3 | 25 | 56.1 | 2.2 | 1.0 | |
| A-4 | 3 | 25 | 69.8 | 2.8 | 1.0 | |
| A-5 | 3 | 25 | 50.0 | 2.0 | 1.0 | |
| A-6 | 2 | 25 | 29.0 | 1.2 | 1.0 | |
| B | 8 | 25 | 250.0 | 10.0 | 1.0 | |
| C | 3 | 25 | 250.0 | 10.0 | 1.0 | No steel fibres |
| D-1 | 2 | 50 | 62.5 | 1.3 | 0.5 | |
| D-2 | 2 | 50 | 100.0 | 2.0 | 0.5 | |
| F | 3 | 25 | 250.0 | 10.0 | 1.0 | One layer of reinforcement |
| G-1 | 2 | 50 | 100.0 | 2.0 | 0.5 | One layer of reinforcement |
| G-2 | 1 | 50 | 250.0 | 5.0 | 0.5 | |
| H-1 | 2 | 50 | 100.0 | 2.0 | 0.5 | Two layers of reinforcement |
| H-2 | 1 | 50 | 250.0 | 5.0 | 0.5 | |
| $\sum$ | 46 | | | | | |

The specimens of type F, G and H are reinforced with meshes of deformed bars. These bars have a nominal diameter of 5 mm and a yield strength of 550 MPa. In table 3 a survey of the layers is shown. The distance between the centers of the bars in the quadratic mesh is given.

Table 3. Distance between reinforcement bars in upper and lower layer respectively.

| | | Type F | Type G | Type H |
|---|---|---|---|---|
| Upper layer | (mm) | – | – | 15 |
| Lower layer | (mm) | 15 | 30 | 30 |
| Punching depth $h$ | (mm) | 25 | 50 | 50 |

The lower layers of reinforcement are placed with a concrete cover of 6 mm from the underside of the slabs and the upper layers with 6 mm cover from the loading cylinder, c.f. figure 5.

### 3.3 Test results

For each test the ultimative punching shear load $P_u$ is determined as the peak value on the $P - \Delta$ relationship, where $\Delta$ is the movement of the loading cylinder.

In this section $P_u$ is analysed and a theoretical model is proposed.

The tests show that the fibres are significant for the punching shear bearing capacity. Comparing the results from test specimens of type B and C the ultimate load is increased with a factor 3.5 when the steel fibres are added.

For test specimens of type F with one layer of reinforcement the ultimate load is increased by 41% compared to the unreinforced specimens of type B. This increase is however misleading because the failure mode is changed significantly by the presence of reinforcement, and therefore (13) cannot be used to predict the ultimate load in this case.

In figure 7 two examples of the failures are shown. For specimens of type F the failure consists of radial cracks, i.e. a bending-like failure, where the layer of reinforcement acts as a membrane in tension.

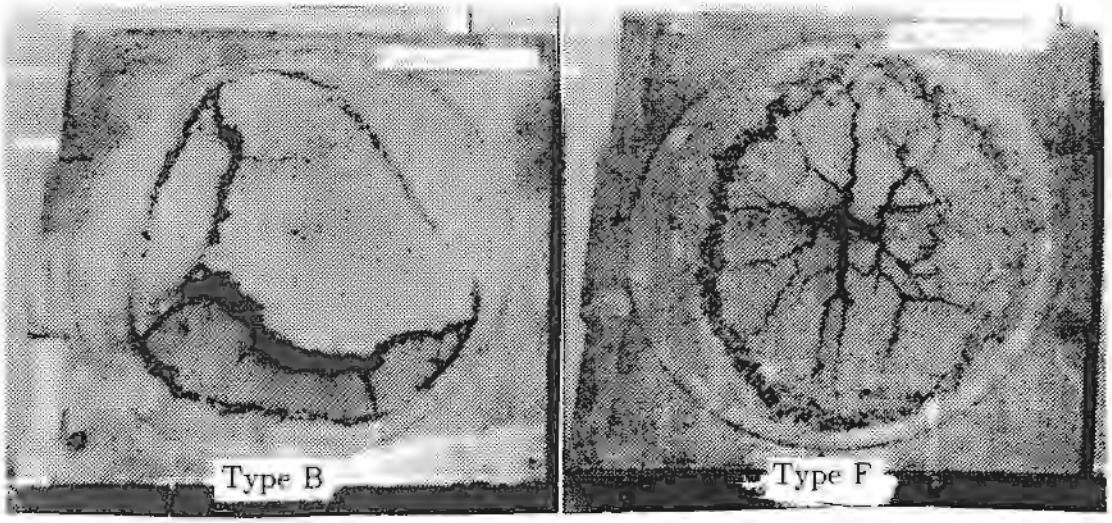


Figure 7: Examples of failure modes for specimens of type B and F.

For the specimens of type G and H with respectively one and two layers of reinforcement and $h = 50$ mm, the failure modes are punching shear. These two types give an increase in ultimate load of 4 and 18% respectively compared to unreinforced slabs.

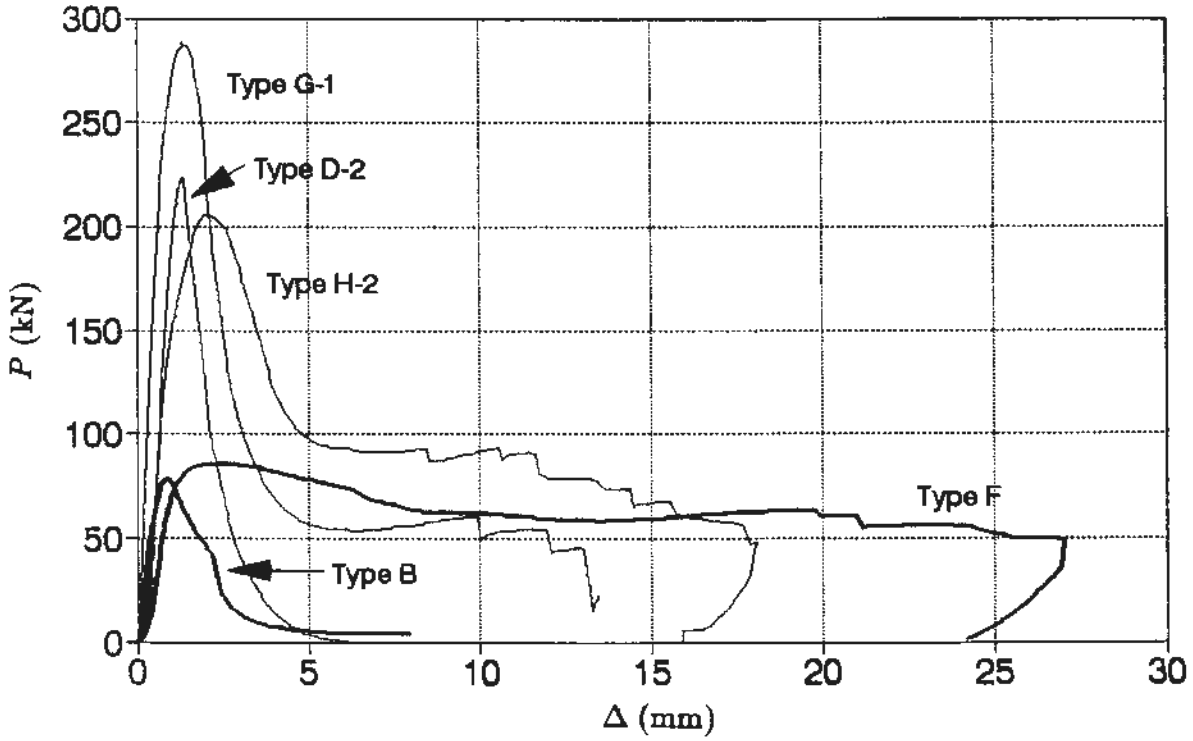


Figure 8: Examples of $P - \Delta$ curves for specimens of type A-1, B, F, G-1 and H-2.

In figure 8 examples of $P - \Delta$ relationship for different test specimens are shown. .

In the following a fitting is performed between the theoretical upper bound solutions and the test results by using the two effectiveness factors $\nu$ and $\rho$, c.f. (8).

The following dimensionless form of the load capacity is used:

$$\frac{P_u}{\pi h^2(2 + d/h)f_c} \tag{14}$$

It is calculated as a constant formal shear stress acting on the cylindrical surface with diameter $(d + 2h)$ and height $h$, related to the uniaxial compression strength $f_c$.

The undisturbed punching diameter $d_1$ is examined on the 8 specimens of type B and a fair value of $d_1$ is estimated to 170-180 mm giving $d_1/h \approx 7$.

If the value $\rho/\nu = 0.005$ is used in (10) we get $K = 43.41$. By solving (12) with $K = 43.41$ and $d/h = 1$ the value $d_1/h = 6.85$ ($\approx 7$) is obtained.

Now a value for $\nu$ is estimated to 0.7 by fitting the test results and the theoretical values using (13). This gives the following estimates for the effectiveness factors

$$\left.\begin{array}{r} \nu = 0.7 \\ \rho/\nu = 0.005 \end{array}\right\} \Rightarrow \rho = 0.0035 \tag{15}$$

In figure 9 the mean values of the test results are plotted together with the upper bound solution for both $d/h = 1$ and $d/h = 0.5$ with varying $D/h$.

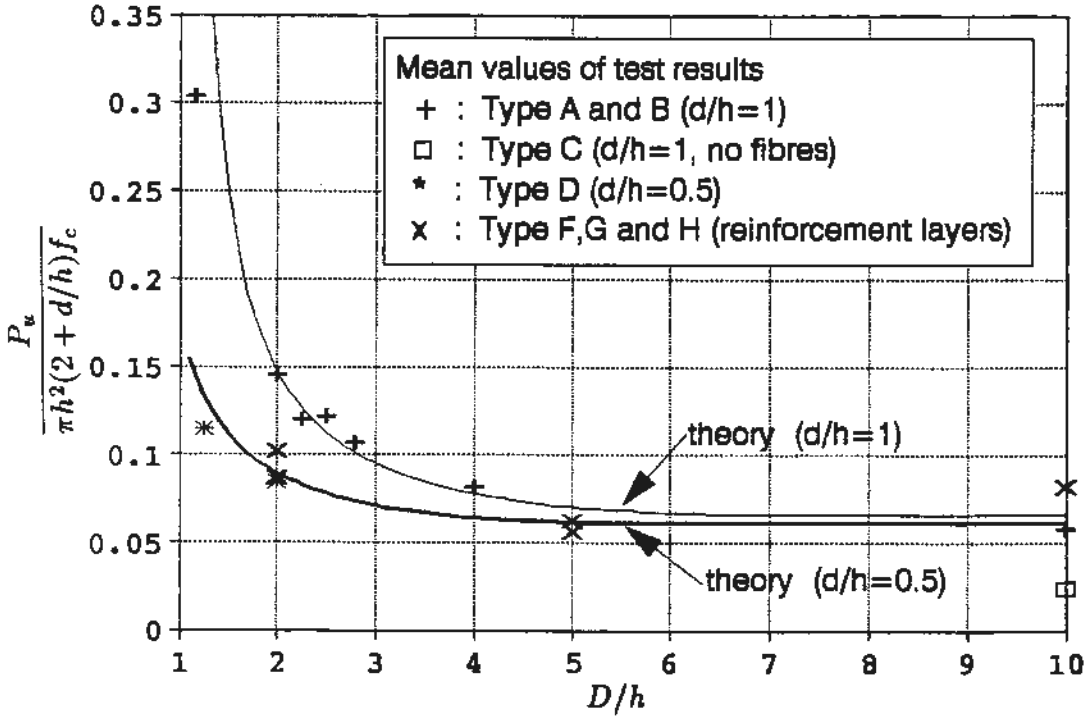


Figure 9: Test results and theoretical punching shear capacity for $\nu = 0.7$, $\rho = 0.0035$ and $\rho/\nu = 0.005$.

Figure 9 shows that the ultimate load increases very fast when the ratio $D/h$ decreases below 2.

The deviations between test and theory are largest for small values of $D/h$. For $D/h = 1.2$ and $d/h = 1$ the theoretical value is bigger than the test result by a factor 2.2 and the same tendency is seen for $d/h = 0.5$. Therefore, it is concluded that the theoretical model should not be used for $D/h < 2$.

To get an idea of the uncertainty of the theoretical model and the test results the standard deviations and the coefficients of variation are calculated.

The coefficients of variation for the test results illustrated in figure 9 vary from less than 1% to about 16%. The highest values are obtained for specimens of type A-2 ($v = 15.6\%$), type A-4 ($v = 11.9\%$) and type B ($v = 15.7\%$) while the other types have $v < 5\%$. These relatively high values of $v$ are however not surprising since similar values are normal in LOK-tests, see /14/.

For $d/h = 1$ the square root of the mean square difference between results from theory and tests is calculated to $6.5 \cdot 10^{-3}$. This value is obtained by leaving out the results for specimens of type A-6 ($D/h = 1.2$), type C (no fibres) and type F (one layer of reinforcement). The value $6.5 \cdot 10^{-3}$ is of the same magnitude as the standard deviations for the test results indicating that the proposed model is sufficiently accurate.

To compare the proposed model with upper bound values normally used for punching shear in ordinary concrete slabs the values of $\nu$ and $\rho$ are calculated for an ordinary concrete with $f_c = 30$ MPa.

According to /7/ p. 376, $\nu$ is given by $\nu = 4.22/\sqrt{f_c} = 0.77$ and $\rho/\nu = 0.0025$ giving $\rho = 0.0019$.

For the COMPRESIT matrix we propose $\nu = 0.7$, $\rho = 0.0035$ and $\rho/\nu = 0.005$, see (15).

The above indicates that the plastic behaviour of COMPRESIT matrix in punching shear is directly comparable to that of ordinary concrete in spite of the compression strength being much higher. Furthermore the fibres result in an effective tensile strength that is worth taking into consideration contrary to what is normally done for ordinary concrete.

## 4. FINAL COMMENTS

This paper deals with triaxial compression tests and punching shear tests on slabs.

The material of the test specimens is the COMPRESIT matrix.

The triaxial tests show that the Coulomb failure criterion with $\varphi = 37°$ is appropriate as failure criterion for the COMPRESIT matrix. The results show a pattern indicating that a more advanced criterion should be used, but it requires more tests to verify this.

The punching shear test show that the theory of plasticity can be used to predict the punching shear bearing capacity of the COMPRESIT matrix in spite of the very high compressive strength in the cement-based material. The steel fibres provide the matrix with considerable ductility and cause that the tensile strength is worth taking into consideration when the bearing capacity is calculated.

## 5. ACKNOWLEDGEMENTS

The research presented in this paper is a part of the EUREKA PROJECT EU264 – COMPRESIT which is partly financed by the Danish and the British governments.

The EUREKA PROJECT EU264 – COMPRESIT is carried out as a collaboration between the following companies and research institutes:
AALBORG PORTLAND A/S, DENSIT A/S Aalborg, NORDJYSK UDVIKLINGSCENTER NUC Aalborg, FORCE INSTITUTES CORROSION DEPARTMENT Brøndby, UNIVERSITY OF LEEDS INDUSTRIAL SERVICES LTD. and CEMENTATION
MINING LIMITED Doncaster UK.

## 6. LIST OF SYMBOLS

$c$ : cohesion

$d$ : diameter of loading cylinder

$D$ : diameter of counter pressure ring

$d_1$ : punching shear diameter

$f_c$ : uniaxial compression strength

$f_c'$ : effective plastic uniaxial compression strength

$f_t'$ : effective plastic uniaxial tensile strength

$h$ : punching shear depth
$k$ : dimensionless constant
$K$ : dimensionless constant
$P$ : compressive load
$P_u$ : ultimate compression load
$r$ : coordinate in the failure surface
$s$ : standard deviation
$v$ : coefficient of variation
$x$ : coordinate in the failure surface
$\alpha$ : angle
$\Delta$ : recorded movement of the loading cylinder
$\nu$ : effectiveness factor to the compressive strength
$\varphi$ : friction angle
$\rho$ : effectiveness factor to the tensile strength
$\sigma$ : normal stress
$\sigma_1$ : first principal stress
$\sigma_2$ : second principal stress
$\sigma_3$ : third principal stress
$\tau$ : shear stress

## 7. REFERENCES

/1/ Bache, H. H., "Compact Reinforced Composite. Basic Principles", Aalborg Portland, Cement- og Betonlaboratoriet, CBL Report No. 41, 1987.

/2/ United States Patent No. 4,979,992, Compact Reinforced Composite, Dec. 25, 1990. H.H. Bache, Aalborg Portland A/S.

/3/ Bache, H. H., "The New Strong Cements: Their Use in Structures", Physics in Technology, Vol. 19, No. 2, March 1988.

/4/ Bache, H. H., "Introduction to Compact Reinforced Composite", Nordic Concrete Research. Publication No. 6, 1987.

/5/ Heshe, G., "Eksperimentelle undersøgelser vedrørende Compact Reinforced Composite (CRC)", Aalborg Portland, Cement- og Betonlaboratoriet, CBL Report No. 45, 1988.

/6/ Heshe, G., "Experimental Research on Compact Reinforced Composite (CRC)", Bygningsstatiske meddelelser, Vol. 59, No. 1, 1988.

/7/ Nielsen, M. P., "Limit Analysis and Concrete Plasticity", Prentice-Hall, Inc., Englewood Cliffs, New Jersey, 1984.

/8/ Dahl, K. B. Kaare, "The Calibration and Use of a Triaxial Cell", Series R.

Department of Structural Engineering. Technical University of Denmark. Not yet published.

/9/ Dahl, K. B. Kaare, "Preliminary State-of-the-art Report on Multiaxial Strength of Concrete", Series R, No. 262, Department of Structural Engineering, Technical University of Denmark, 1990.

/10/ Heshe, Gert & Nielsen, Claus V., "EU264 - COMPRESIT, Technical Report, Subtask 1.4 – Behaviour in Compression", Nordjysk Udviklingscenter NUC, Aalborg. Not yet published.

/11/ Heshe, Gert & Nielsen, Claus V., "EU264 – COMPRESIT, Technical Report, Subtask 1.5 – Behaviour in Shear", Nordjysk Udviklingscenter NUC, Aalborg. Not yet published.

/12/ Jiang, D. & Shen, J., "Strength of Concrete Slabs in Punching Shear", Journal of Structural Engineering, vol. 112, No. 12, 1986.

/13/ DS 423.31, "Testing of Concrete – Hardened Concrete – Pull-out Strength", 1. ed., March 1984.

/14/ Krenchel, Herbert & Bickley, John A., "Pull out Testing of Concrete". Nordic Concrete Research Publication No. 6, 1987.

/15/ Richart, F.E., Brandtzaeg, A. & Brown, R.L., "A Study of the Failure of Concrete under Combined Compressive Stresses". Bulletin No. 185, Engineering Experiment Station, University of Illinois, Urbana 1928.